Phase transition analysis of ammonia-water mixture at high pressure and low temperature

Alessio Cargioli, University of Pisa, Italy

Supervisors: Dr. Konstantin Glazyrin, Dr. Anna Pakhomova

September 3, 2019

Abstract

The studies of ammonia hydrates have become of high relevance due to their implications for the geophysics of icy moons in the solar system. We investigated the phase diagram of a 33% water-ammonia mixture with usage of a cold finger cryostat for cooling down the sample and a diamond anvil cell for increasing the pressure. Before the in situ x-ray diffraction measurements a calibration of the cryostat sensors was performed. Here we report on results of the calibration and in situ HP-LT experiment.

Contents

1 Introduction

The study of mixtures of water and ammonia has become of interest mainly for two reasons. The first one is that it is a simple mixture which presents mixed hydrogen bonds which are hydrogen bonds between an acceptor atom which is part of one molecule, such as a water molecule, with a donor atom from a different type of molecule, such as an ammonia molecule. Studying their properties could help to understand better the properties of more complex molecules, for example the DNA[1].
The second motivation concerns the internal structure of icy moons as Titan, Europa and Callisto. In particular measurements conducted by the Cassini space-craft on the gravitational quadrupole of Titan suggested that the moon is less denser then expected. This fact brought to confirm the suspect that under the ice surface there is an ocean of water and ammonia[2] which could potentially host life. One of the possible internal structures of Titan is reported in Fig.1.

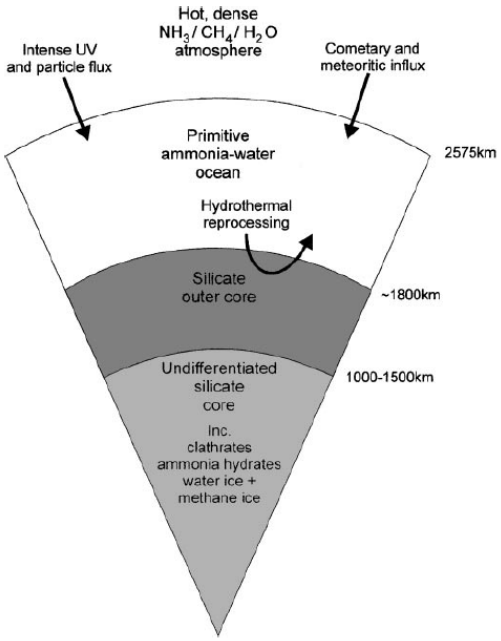

Figure 1: Possible internal structure of Titan [3]

Six parameters can influence the development of primordial life on Titan: temperature, pressure, pH, viscosity, nutrient availability and energy availability. The possibility of the development of simple bacterias in Titan's interior can not be excluded. Thus, the temperature in the ocean is estimated to be between 235 and 240K, while in an isolated hypersaline lake in Antarctica a *Desolfovibrio* bacteria at the temperature of 222K[3] has been found. In addition the possible existence of cryogenic activity under the moon's surface, would favor the formation of some small heavens for this kind of life-forms.
For these reasons it is necessary to accurately know the properties of water-ammonia

mixtures under P-T conditions relevant for interiors of icy moons.

When water and ammonia are mixed together they can form different types of mixtures depending of the ratio of the two molecules. We can distinguish three different stoichiometric compounds: ammonia monohydrate($NH_3 \cdot H_2O$), ammonia dihydrate ($NH_3 \cdot 2H_2O$) and ammonia hemihydrate ($2NH_3 \cdot H_2O$). At non-ambient conditions ammonia hydrates are known to reveal rich polymorphism[4] (Fig.2a-2b).

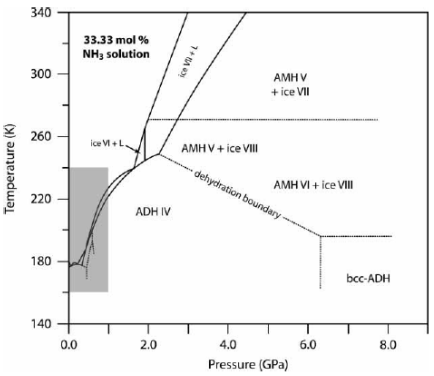

Figure 2a: Phase diagram of ammonia hydrates

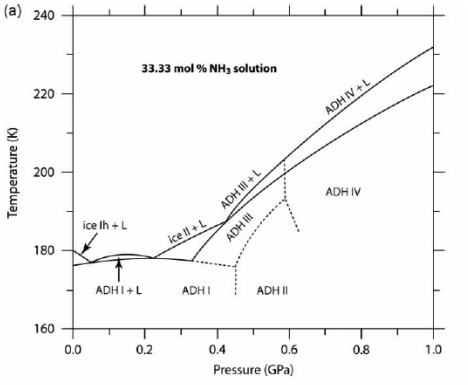

Figure 2b: Phase diagram 0-1GPa

Several studies have been performed on these compounds and they are well reviewed in the chapter 1.8 of C.W. Wilson's PhD. thesis [1]. Table 1 summarizes the known information of characterized ammonia hydrates.

Phase	Symmetry	a [Å]	b [Å]	c [Å]	β [°]	Space Group	P-T condition	Source
ADH I	Cubic	7.1278(8)	-	-	-	$P2_13$	P=atm, T=150K	[4]
ADH II	Monoclinic	6.07465(16)	6.72577(14)	7.78334(17)	102.1065(19)	$P2_1/n$	P=174MPa, T=174K	[5]
AMH I	Orthorombic	4.5108(14)	5.58691(20)	9.71452(34)	-	$P2_12_12_1$	P=atm, T=113K	[1]
AMH II	Orthorombic	18.8285(4)	6.94145(16)	6.84492(16)	-	Pbca	P=atm, T=180K	[6]
AMH VI	Cubic	3.2727(2)	-	-	-	$Im\bar{3}m$	P=6.5GPa, T=300K	[7]
AHH I	Orthorombic	4.51(1)	5.587(3)	9.700(5)	-	$P2_12_12_1$	P=6.5GPa, T=300K	[8]
AMH V=AHH II	Monoclinic	3.358(4)	9.215(1)	8.933(1)	94.331(8)	$P2_1c$	P=3.5GPa, T=300K	[1]

Table 1: Unit cell parameters of known phases

Despite the extensive research, there are still open questions on ammonia-water phase diagram. Thus ADH IV has not been structurally characterized yet. ADH II is supposed to be the one reported in the table but Fortes[4] underlines that it doesn't satisfy all the diffraction peaks. In addition let's point out that in the phase diagram it's reported the phase AMH V, but after the study of Wilson it has been better characterized as AHH II.
The aim of this project is to explore the phase diagram of 33% water-ammonia mixture under conditions relevant to the interior of icy satellites. As previous studies are limited to in situ powder XRD, our particular goal is to perform single crystal X-Ray diffraction (SCXRD) on the crystals grown under HP-LT conditions.

2 Theory

2.1 X-Ray diffraction

X-ray diffraction is one of the most used techniques to solve the internal structure of materials. It uses the Bragg's law (eq.1) (or the Laue construction) which creates a direct connection between the crystal structure of the sample and its reciprocal space.

$$2dsin(\theta) = n\lambda \tag{1}$$

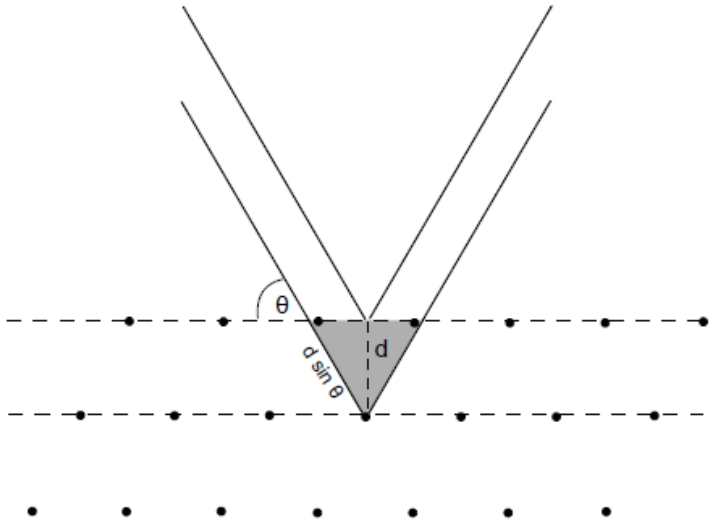

Figure 3: Schematic of diffraction condition on a crystal

In Fig.3 d is the distance between the crystal planes, λ is the wavelength of the incident beam, n is the order of diffraction and θ the incident angle (the scattering angle is usually indicated with 2θ). The simple equation 1 shows how the only important directions for identifying the crystal planes are the ones which can create constructive interference of the scattered light.

We can also distinguish two kinds of diffraction depending on the texture of the sample: single crystal diffraction and powder diffraction. A typical measurements of the first type is reported on the left in Fig.4 taken from a measurement on lawsonite ($CaAl_2Si_2O_7(OH)_2 \cdot H_2O$), while on the right there is an example of powder diffraction of water ice VI.
In the powder measurements we lose the angular information of the diffraction pattern due to different orientations of the small crystals in the sample (more the distribution is uniform more the rings are well defined). On the contrary; in the single crystal patterns we have angular information for every collected reflection that can potentially provide

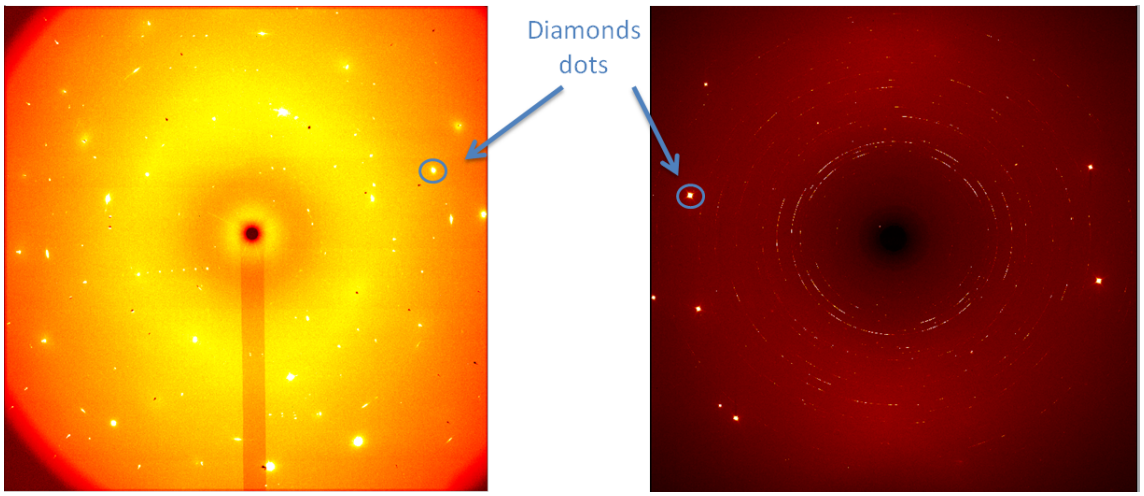

Figure 4: Examples of SCXRD on the left and powder diffraction on the right

better insight into internal atomic structure. In general, even though the ideal case would be to have always a single crystal as a sample, it is not always possible to obtain. For example in this report we will show how the crystallization of the desired phases was difficult and in most of the cases the formation of amorphous materials was observed. In addition, using a DAC as sample chamber diffraction patterns are always contaminated with diamonds single crystal reflections (Fig.4) which luckily are well known and not difficult to mask.

3 Methodology

In order to explore the phase diagram of a specific compound a control over the pressure and the temperature is needed. Modern techniques allow to cover large area of P-T space: up to TPa in pressure and from 5 to 1000K in temperature. In our report we focus on the region between 3-4GPa and 180-300K. The techniques for high-pressure and low temperature generation will be introduced in following sections 3.1 and 3.2 respectively.

3.1 Diamond anvil cell technique and preparation of the sample

3.1.1 General description

The operation principle of a diamond anvil cell (DAC) consists on placing the sample between two cut diamonds which can be pushed together mechanically. A simple schematic is shown in Figure 5.
The diamonds are fixed by glue to their metal container by which the pressure can be increased using 4 screws. To fix the sample between the diamonds, and also to avoid their breaking due to the high pressure, a metallic gasket is placed as in Fig.5. In our case the

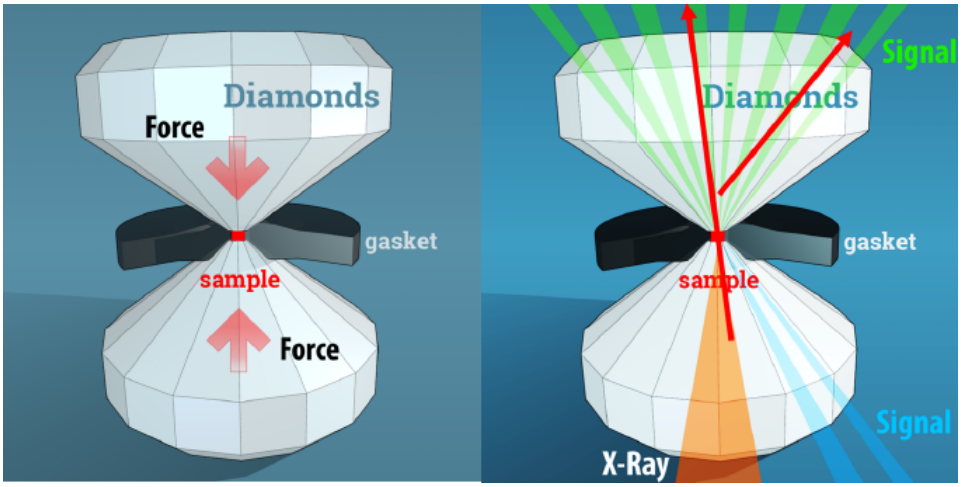

Figure 5: Schematic for diamond anvil cell

material of the gasket is rhenium, but beryllium and steal are also used depending on the goal of the measurement. In addition, depending on the kind of sample, a pressure medium like neon or helium can be needed to guarantee an homogeneous compression. This technique is used in particular for crystals at room temperature.

The use of the diamonds to increase the pressure has the advantage of being able to reach quite high pressures in a relative simple way; on the other hand their presence influence the diffraction measurements. In fact they also are crystals so they produce a diffraction patter which is however very well known, in this way they can be excluded from the data.

A way of measuring the pressure inside the sample chamber is also needed. One technique consists in placing rubies in the chamber and measuring the wavelength of the emitted fluorescence light when they are hit by a laser. The ruby fluorescence spectrum is well known and by measuring the shift in the wavelength at ambient pressure the pressure in the chamber can be calculated.

3.1.2 Preparation of the sample

As already explained, the goal of the experiment is to investigate phase transitions of a 33% water-ammonia mixture. In order to lead the liquid sample into a DAC the following procedure was followed:

1. **indentation of the rhenium gasket**: 200μm thick gasket is placed between the diamonds and compressed up to $\simeq$22GPa. As a result, the gasket is indented to $\simeq 30 - 40\mu$m.

2. **drilling of the gasket**:the indentation was drilled through in the center by a copper wire of 200μm of diameter in order to produce a sample chamber.

3. **cleaning of the gasket and diamonds from impurities**: it is usually made with tampons imbued in isopropanol or ethanol.

4. **placement of the gasket on the diamond**: we usually use some plasticine to fix the gasket in the correct position.

5. **loading of rubies in the cell**: rubies of 10-20μm diameter were placed in the sample chamber, on the culet of the diamond with the help of a needle.

6. **loading of the water-ammonia mixture**: it is loaded in the cell with the help of a syringe under the fume hood to avoid the strong smell due to the ammonia. This procedure is particularly delicate because the mixture tends to evaporate quickly, for this reason the closure of the cell must be fast. In addition, because the sample is liquid, there is the risk to lose the rubies; for this reason we usually several of them to ensure that at least one remains inside the sample chamber after loading.

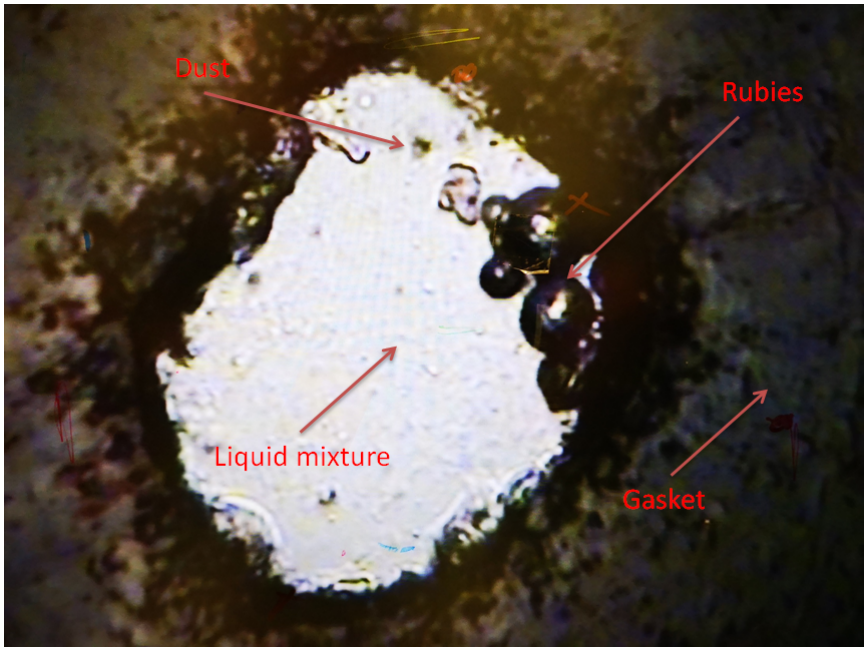

Figure 6: Microscope picture of the sample

After the loading the sample chamber looks at the microscope as in Fig.6. If the sample is liquid at ambient conditions, as in our case, it is sometimes difficult to understand if the loading was successful. One on the signal that there is liquid in the cell is the presence of Brownian motion of some dust particles which can remain on the surface of the diamonds. However the presence of liquid does not necessary imply the presence of ammonia in the sample due to possible evaporation. One way of understanding if some ammonia remained is by XRD analysis of crystallized phase or by Raman spectroscopy.

3.2 Cryostat

3.2.1 Cryostat description

To cool down the sample a cold finger cryostat has been used. It uses liquid helium injected in a hollow cylinder installed on the top of the chamber where the DAC is located(Fig.7-8). In order to keep the temperature stable in the holder three heaters are installed in its the upper part. In addition, to keep as low as possible the exchange of heat with the environment, the holder in Fig.8 is placed in a vacuum chamber(Fig.9) where pressure reaches around 10^{-6}bar.

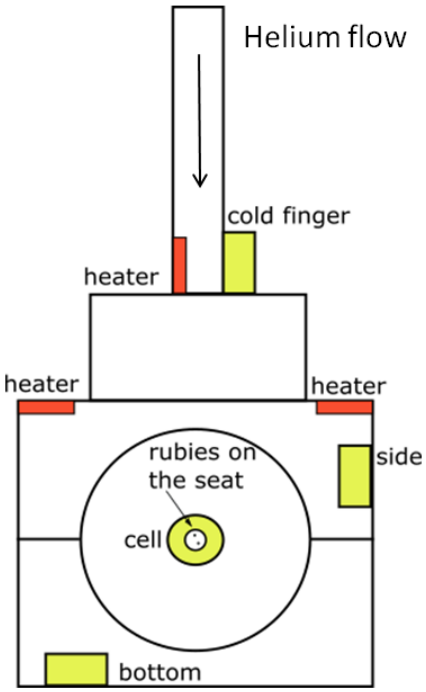

Figure 7: Simple schematic of the DAC holder

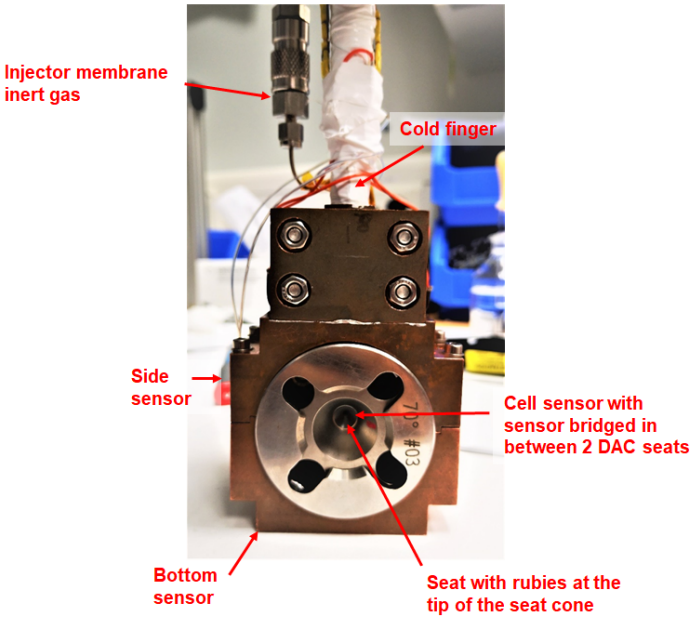

Figure 8: DAC installed in the holder

To increase the pressure of the cell the screws can not be used anymore because the cell is isolated from the environment. For this reason the DAC is installed in another metallic holder equipped with a membrane (Fig.10). By injecting gas into the membrane it expands and pushes the two parts of DAC closer to each other and finally increases the pressure in the sample chamber.
Typically 3 sensors are located in the holder as in Fig.7 in order to monitor the temperature. In first approximation the temperature of the cell is homogeneous, however this assumption has not been proved experimentally. Therefore to ensure the precise temperature estimation, we set up the goal to perform cryostat calibration.

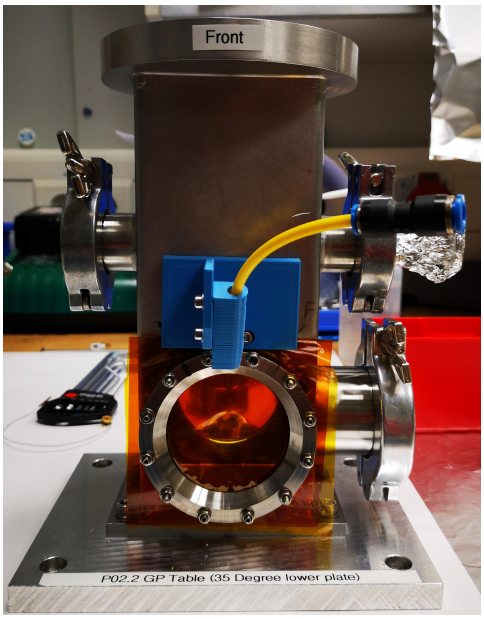

Figure 9: Vacuum chamber

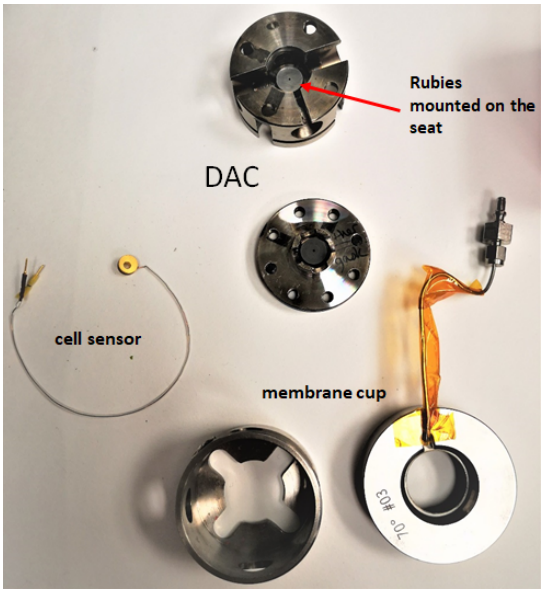

Figure 10: DAC, sensor, membrane

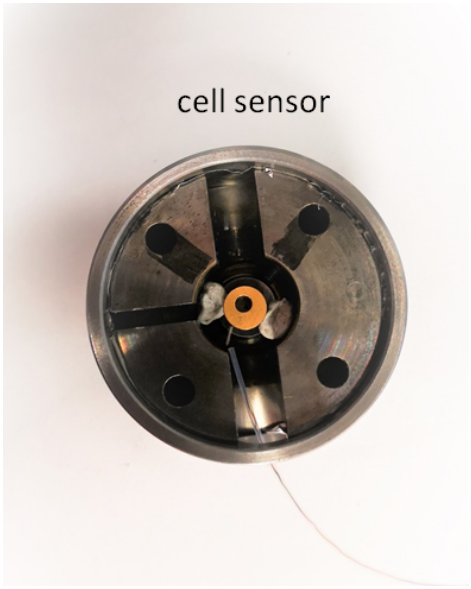

Figure 11: Sensor installed in the cell

3.2.2 Cryostat calibration

In order to understand how well is the agreement from the measurements between the 3 side sensors and the real temperature in the sample chamber, we installed a sensor on the DAC seat with 2 rubies. Rubies have a well characterized fluorescence spectrum which is T dependent. There are several reports concerning rubies as T calibrant[9]-[10] and our additional goal was to check their consistency with our measurement.We expect

the cold finger sensor to be the less reliable because of its very close position to the flux of liquid helium. For this reason we mostly use T_{side} or T_{bottom} as comparison with T_{cell}.

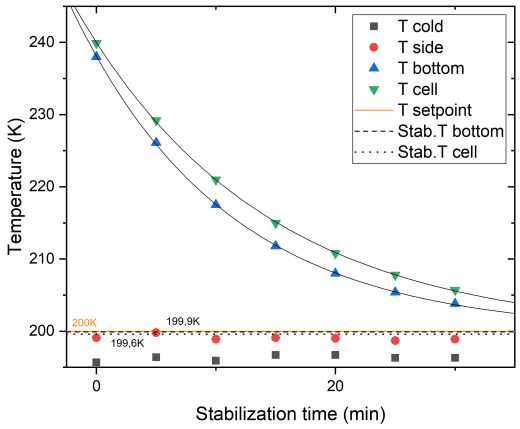

Figure 12: Stabilization curves 200K

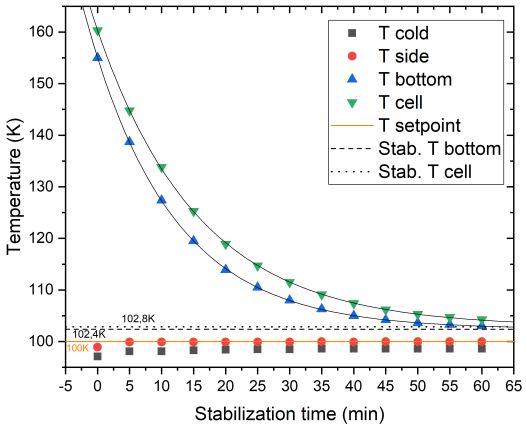

Figure 13: Stabilization curves 100K

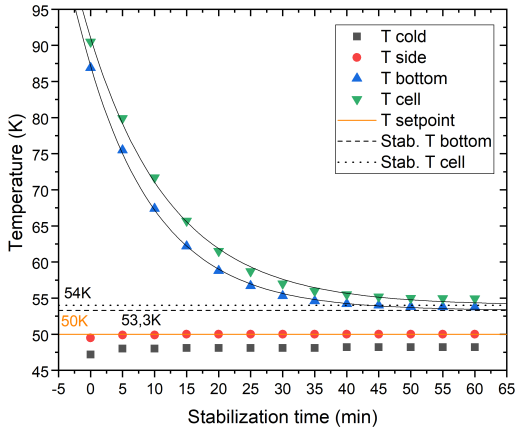

Figure 14: Stabilization curves 50K

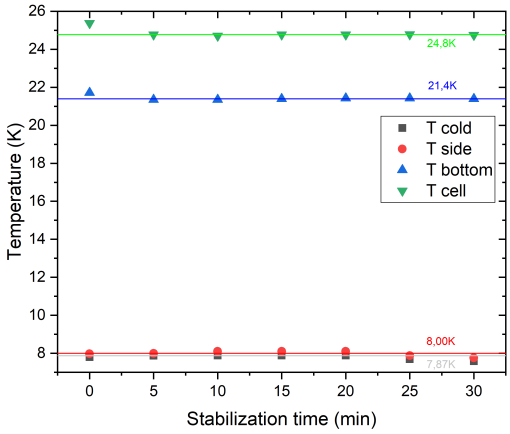

Figure 15: Stabilization curves 8K

After every cool down T_{side} and T_{cold} took a short time to reach the set temperature, on the contrary T_{bottom} and T_{cell}, due to their position, needed from 30 minutes to 1 hour of stabilization time (starting to count from the moment when the other 2 sensors are stabilized). For 200,100,50 and 8K we recorded the time dependent trend of the temperature by taking a measure every 5 minutes. These acquisitions are reported in Fig.[12-15]. As we could expect T_{side} and T_{cold} are stable for all the time range while T_{bottom} and T_{cell} demonstrate an exponential decay; only the case of 8K is an exception.

From Fig.16-17 we can assume T_{bottom} a good estimation of T_{cell} with a systematic un-

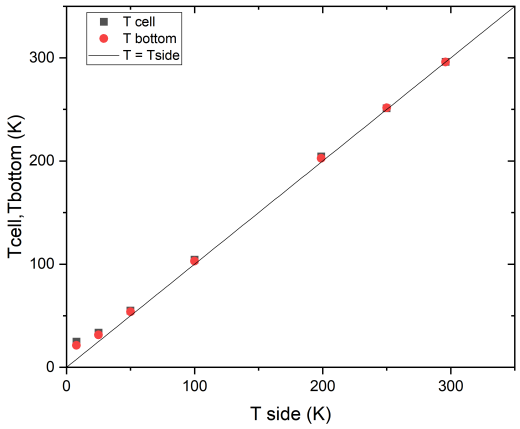

Figure 16: T_{cell}, T_{bottom} vs T_{side}

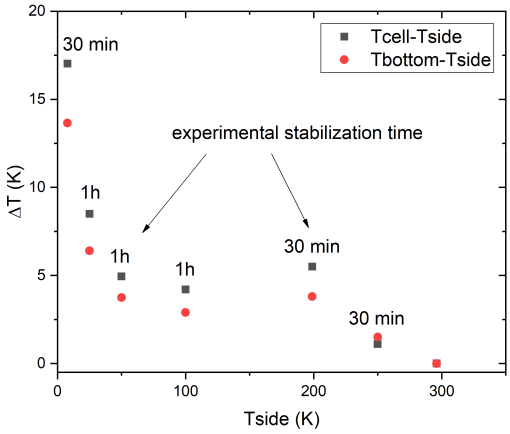

Figure 17: $T_{cell} - T_{side}$,$T_{bottom} - T_{side}$ vs T_{side}

derestimation around 2-5K for temperatures under 200K. In addition T_{side} is a good estimation of all our set-points (while as expected T_{cold} is always an underestimation). For temperatures above 50K T_{cell} reaches the set T within a range of 5K. Below 50K the cryostat starts to present some limitations, in particular, as shown in Fig.15 the lowest temperature achievable in the cell is 24.8K against the 8K taken as set-point and reached by T_{side}. This fact could be due to the not perfect vacuum present in the chamber. Even if we have a pressure around 10^{-6}bar it may not be enough to prevent the heat exchange with the environment.

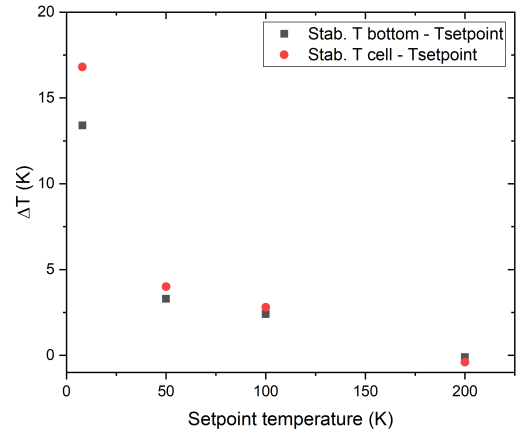

Figure 18: Stab.$T_{bottom} - T_{setpoint}$,Stab.$T_{cell} - T_{setpoint}$ vs $T_{setpoint}$

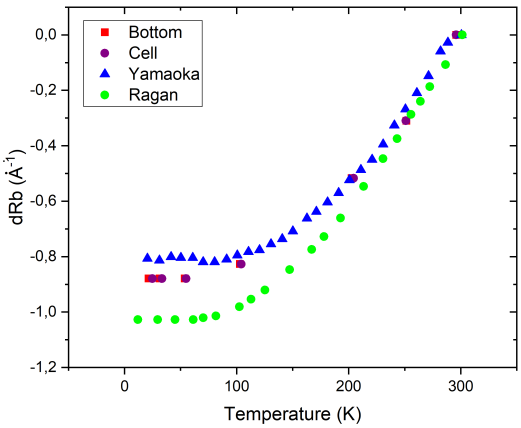

Figure 19: Wavelength shift from our and literature data

From the fit of the exponential decay of T_{cell} and T_{bottom} the respective asymptotic tem-

peratures were extracted and compared with the relative set-point as shown in Fig.18. As well as for the measured stabilization temperature there is a drift in the asymptotic value while we decrease the set-point. This effect could be compensated by adjusting the set-point in a way to reach the set temperature. In general if we stay above 25K (this fit is not present because we did not take any data due to time limitation) this offset is within 5K.

Lastly we calculated the difference in the ruby fluorescence emission between the wavelength at room temperature and the different reached temperature. The result is the plot in Fig.19 which shows a big discrepancy between our data and the data from the literature. The conclusion is that we can not use data from the literature to calibrate our experiment and to measure the pressure-temperature because it is batch dependent. To achieve a good measure we need to make this measurement every time at least if we want to reach temperature below 150-100K.

3.3 X-Ray diffraction experiment

In situ high-pressure diffraction experiments were performed at the experimental station P02.2 (Extreme Conditions Beamline) at synchrotron Petra III (Hamburg, Germany). Monochromatic X-ray diffraction experiments were performed using X-rays with wavelength of 0.2905 Å. The X-ray beam was focused by Compound Reflective Lenses to $8{\times}3\ \mu m^2$. Diffraction patterns were collected using Perkin Elmer detector.The detector-sample distance was calibrated with a CeO_2 standard using the procedure implemented in the program Dioptas, used also for the data analysis. At each pressure-temperature point either a wide-scan, a stepped ω-scan or a grid of still images were collected. Wide-scans consisted of 40 s exposures during rotations of $\pm 20^\circ$ of the DAC. Step scans consisted of individual exposures taken over 0.5° intervals to constrain the ω angle of maximum intensity of each peak. Three grids were collected with the specifics shown in Tab.2.

P[GPa]	T[K]	cells number [z·y]	Step [μm]
3-4	181	13·19	5
3-4	240	9·9	7
3.15	300	11·11	7

Table 2: Grid specifics

4 Results

After setting the pressure between 3 and 4 GPa we tried to explore different crystal phases by cooling the sample down and warming it up.

- **T = 204K, Phase expected = ADH IV** After the cool down the formation of ice in the microscope was not observed. The acquired diffraction pattern possessed only diamonds reflections. This indicates the presence of an amorphous phase.

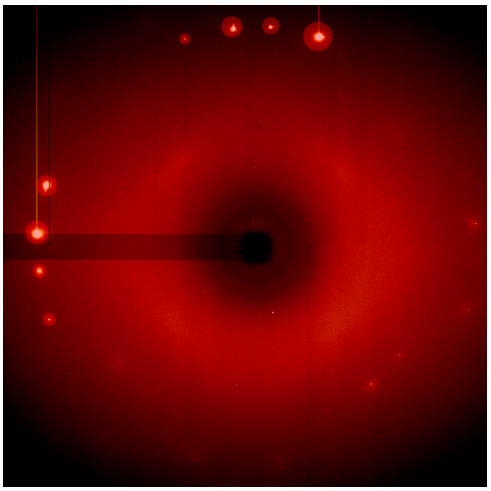

Figure 20: Amorphous phase 204K

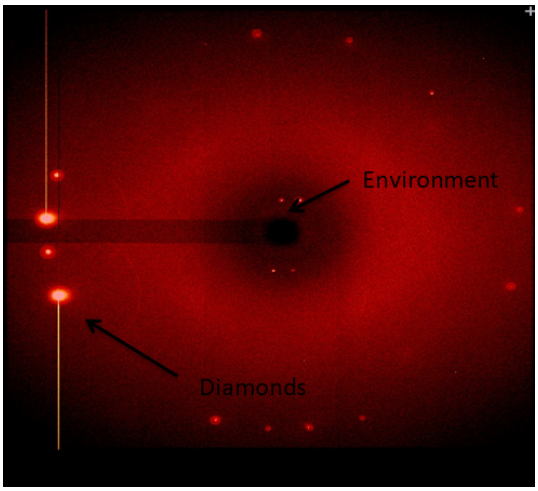

Figure 21: Amorphous phase 181K

In Fig.21, besides the diamond reflections, there are also 4 central dots. We assume they originate from the environment as they are present unchanged in other measurements.

- **T = 181K, Phase expected = ADH IV** Upon cooling down, no optical change in the sample chamber has been noticed. In order to check whether the amorphous phase was present in every part of the sample we performed a grid measurement (Tab.2).

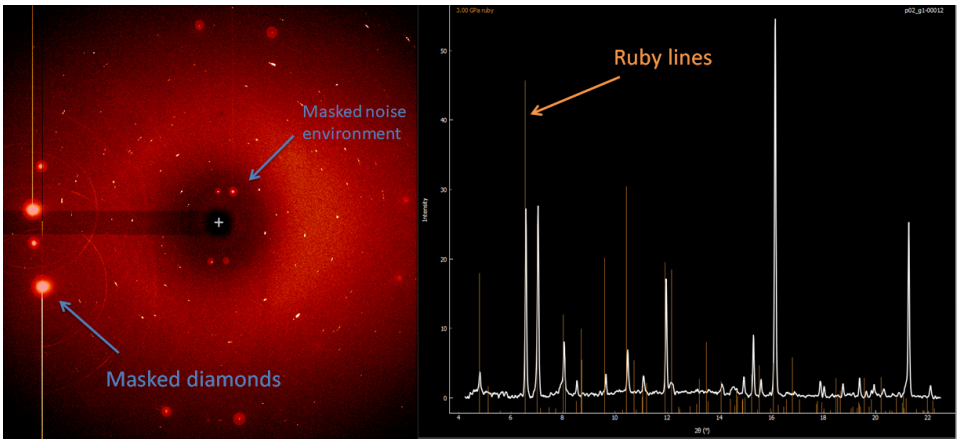

Figure 22: Ruby diffraction pattern and integrated intensities

That allowed us to conclude that an amorphous phase was present in the most part of the sample. The only non trivial signal was found in the upper part of

the grid as shown in Fig.22. By the comparison with the known ruby diffraction pattern and because ruby spheres were located near that cells we assume that signal originates from rubies. There is only one exception for 2 frames with wide diffraction lines which do not belong to rubies. However, these peaks did not match any other known phase.

- **T = 240K Phase expected = ADH IV or AHH II + ice VIII** At this point the crystallization of ice has not been optically observed. A grid has been performed again in order to detect micro-crystals in the sample.

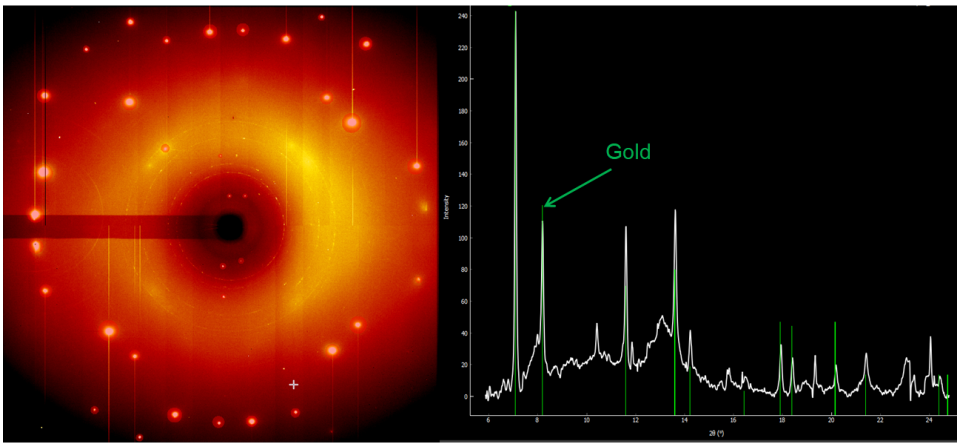

Figure 23: Diffraction pattern from gold or unknown FCC phase

Some wide circles have been detected and compared with known diffraction patterns (Fig.23). The analysis shows that gold may be present in the sample even if we suppose a contamination during the loading procedure of this element unlikely. In fact there are no reasons to believe that gold was present in any kind of object used for the sample preparation. For this reason it is not to exclude the formation of an unknown FCC crystal phase in the sample with an expected side around 4 Å. The comparison was also made with NH_3 III which also has a cubic structure but its unit cell is too big to explain the measured pattern.

- **P = 3.15GPa, T = 300K, Phase expected = ice VII + L** At this P-T point we saw formation of ice in the microscope (Fig26).A grid measurement was performed to find a large enough single crystal. The sample was neither a good crystal nor a good powder but something in between.

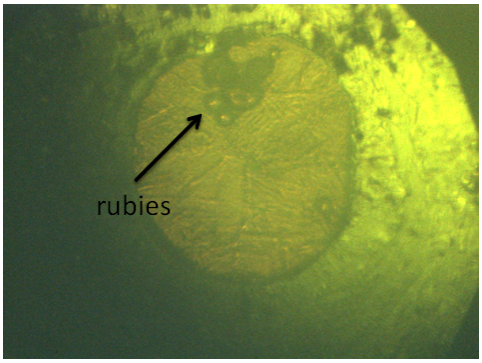

Figure 24: Ice formation in the sample

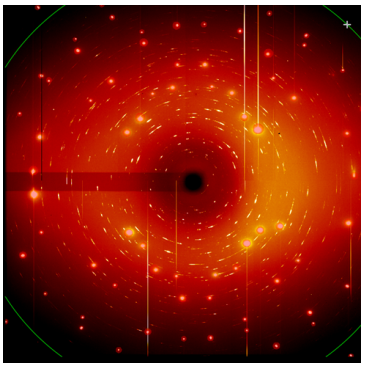

Figure 25: Diffraction pattern from rubies

From the upper part we obtained again the typical patterns of the rubies, while from lower part we found patterns of unknown phase. The sample was crystallized into small crystals, so that we had to treat the data as a powder.

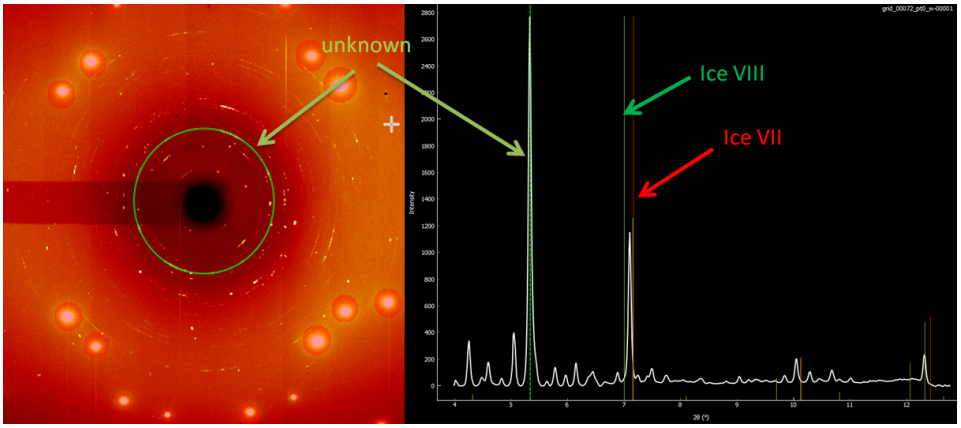

Figure 26: Ice diffraction pattern + unknown intensities

One of the most clear acquisitions is reported in Fig.26. We face the problem to distinguish ice VII from VIII, but on the base of the literature we conclude that ice VII is present in the sample. In addition a new series of lines are present in the intensity plot that do not match with any known spectra [1]. It is not likely for them to be due to environment factors because they are not present as a stable background noise in all the measurements. Because ADH IV phase is not characterized yet, we propose that as unidentified phase.

As summary we report in Tab.3 all the analyzed pressure-temperature points with the conclusions from our measurements.

[1]The intensity comparison has been made with the following compounds from original .cif files: ruby, rhenium, ice VI-VII, gold; and from modified .cif files: ice VIII, ammonia III-IV, AHH II, AMH VI.

P[GPa]	T[K]	Phase expected	Phase measured	XRD images
3-4	204	ADH IV	amorphous	20
3-4	181	ADH IV	amorphous	21
3-4	240	ADH IV or AHH II + ice VIII	gold contamination or unknown cubic phase	23
3.15	300	ice VII + L	ice VII + unknown phase	26

Table 3: Summary of the measured pressure-temperature points

5 Conclusions

The calibration of the cryostat has shown that the temperature in the sample chamber (T_{cell}) is well characterized by the temperature measured by the bottom sensor. Stabilization time from 30 minutes to 1 hour is needed to give time to the temperature in the cell and at the holder bottom to reach their asymptotic values. The lowest temperature achievable for the sample is around 25K compared to the lower temperature of the cold finger around 8K.

In a course of in situ HP-LP diffraction experiments, we managed to observe only an amorphous phase at LT. This observation is in agreement with Fortes[4], who reported the difficulty of crystallization due to the high viscosity of the liquid phase at low temperature. At T above 240K (above the dehydration line of ammonia hydrates) gold was detected. Its presence may be due to a sample contamination during the loading procedure, even if we do not exclude the presence of an unknown FCC crystal phase with the side of the unit cell around 4Å. At room temperature, an unknown phase was found to coexist with ice VII. Further analysis and experiments are needed for the identification of the 2 unknown phases.

Acknowledgments

I would like to thank my supervisors Anna and Konstantin for following in my work with such dedication and for being always available to answer all my doubts and questions. Another thanksgiving is due to Desy and all the people who made this great summer program possible. In the end I need to thank all the recent friends I made during this two months, it was a really interesting and enriching experience working and living with them and I hope I will be able to meet them again in the future.

References

[1] Craig W. Wilson, *High-Pressure Studies of Ammonia Hydrates,* PhD thesis at the University of Edinburgh, October 2013.

[2] A.D. Fortes, *Titan's internal structure and the evolutionary consequences,* Planetary and Space Science, 60 (2012) 10–17.

[3] A.D. Fortes, *Exobiological Implications of a Possible Ammonia–Water Ocean inside Titan,* Icarus 146, 444–452 (2000).

[4] A. D. Fortes , I. G. Wood , M. Alfredsson , L. Vočadlo , K. S. Knight , W.G. Marshall , M. G. Tucker, F. Fernandez-Alonso, *The high-pressure phase diagram of ammonia dihydrate,* High Pressure Research: An International Journal, 27:2, 201-212, DOI: 10.1080/08957950701265029 (http://dx.doi.org/10.1080/08957950701265029).

[5] Griffiths, Gareth I.G.; Fortes, A.Dominic; Pickard, Chris J.; Needs, R.J, *Crystal structure of ammonia dihydrate II,* Journal of Chemical Physics (2012) 136, (17) p174512-1-p174512-9.

[6] Fortes, A.D.; Suard, E.; Lemee-Cailleau, M.H.; Pickard, C.J.; Needs, R.J., *Crystal structure of ammonia monohydrate phase II,* Journal of the American Chemical Society (2009) 131, (37) p13508-p13515.

[7] J. S. Loveday and R. J. Nelmes, *Ammonia Monohydrate VI: A Hydrogen-Bonded Molecular Alloy,* Phys. Rev. Lett. 83, 4329 (1999), ISSN 0031-9007, URL http://link.aps.org/doi/10.1103/PhysRevLett.83. 4329.

[8] I. Olovsson and D. H. Templeton *The Crystal Structure of Ammonia Monohydrate,* Acta Crystallogr. 12, 827(1959), ISSN 0365110X, URL http://scripts.iucr.org/cgi-bin/paper?S0365110X59002419.

[9] Deirdre D. Ragan, R. Gustavsen, and David Schiferl *Calibration of the ruby R1 and R2 fluorescence shifts as a function of temperature from 0 to 600 K,* Journal of Applied Physics 72, 5539 (1992); https://doi.org/10.1063/1.351951 .

[10] Hitoshi Yamaoka, Yumiko Zekko, Ignace Jarrige, Jung-Fu Lin, Nozomu Hiraoka, Hirofumi Ishii, Ku-Ding Tsuei, and Jun'ichiro Mizuki *Ruby pressure scale in a low-temperature diamond anvil cell,* J. Appl. Phys. 112, 124503 (2012); https://doi.org/10.1063/1.4769305 .